The role of martensitic transformation on bimodal grain structure in ultrafine grained AISI 304L stainless steel

S.Sabooni[a]*, F.Karimzadeh[a], M.H.Enayati[a], A.H.W.Ngan[b]

[a]Department of Materials Engineering, Isfahan University of Technology, 84156-83111, Isfahan, Iran

[b]Department of Mechanical Engineering, The University of Hong Kong, Pokfulam Road, Hong Kong, China

Tel: +98 9373875707

Fax: +98 3133912752

Corresponding Author email: s.sabooni@ma.iut.ac.ir

Abstract:

In the present study, metastable AISI 304L austenitic stainless steel samples were subjected to different cold rolling reductions from 70% to 93%, followed by annealing at 700 $^{\circ}$C for 300 min to form ultrafine grained (UFG) austenite with different grain structures. Transmission electron microscopy (TEM) and nanoindentation were used to characterize the martensitic transformation, in order to relate it to the bimodal distribution of the austenite grain size after subsequent annealing. The results showed that the martensite morphology changed from lath type in the 60% rolled sample to a mixture of lath and dislocation-cell types in the higher rolling reductions. Calculation of the Gibbs free energy change during the reversion treatment showed that the reversion mechanism is shear controlled at the annealing temperature and so the morphology of the reverted austenite is completely dependent on the morphology of the deformation induced martensite. It was found the austenite had a bimodal grain size distribution in the 80% rolled and annealed state and this is related to the existence of different types of martensite. Increasing the rolling reduction to 93% followed by annealing caused changing of the grain structure to a monomodal like structure, which was mostly covered with small grains of around 300 nm. The existence of bimodal austenite grain size in the 80% rolled and annealed 304L stainless steel led to the improvement of ductility while maintaining a high tensile strength in comparison with the 93% rolled and annealed sample.

Keywords: Austenitic stainless steel, Bimodal grain size distribution, Lath type martensite, Dislocation cell type martensite, Nanoindentation, Reversion mechanism

1. Introduction:

Thermomechanical processing based on Strain Induced Martensitic (SIM) transformation followed by reversion annealing treatment has been introduced as one of the most important methods for producing ultrafine/nano grained (UFG/NG) austenitic stainless steels [1-6]. Although UFG stainless steels exhibit excellent yield and tensile strength, they sometimes show poor ductility in comparison with coarse-grained counterparts [6]. The increase of yield and tensile strength is due to the well-known Hall-Petch effect [7-8] – experiments have shown that the strength of UFG/NG stainless steels is about 3 to 7 times higher than coarse-grained counterparts [1-5]. However, their ductility, normally uniform elongation during uniaxial tensile test, is low and this drawback can limit their commercialization [9]. In UFG/NG stainless steels, the large amount of grain boundaries can act as nuclei for cracks, which may account for the low ductility [10]. Another important reason can be the localization of plastic deformation [11], since dislocation storage in NG materials is much less efficient as in coarse grained materials, and this results in very weak work hardening of these materials [12]. In fact, tensile tests of most of the UFG/NG steels in the literature revealed relatively flat stress-strain curves in the plastic region without much work hardening [13]. In the past few years, a great deal of research has been performed to improve the ductility of UFG/NG steels based on engineering the grains. Changing the granular structure in NG materials can result in significant modifications to their behavior, and one of the most effective ways to overcome the weak ductility problem in UFG/NG stainless steels is to create a bi- or multi-modal grain size distribution [14]. It has been shown that the formation of a bimodal structure in nano-micro scale can produce a large gain in ductility, with just a small decrease in strength [14]. The existence of bi- or multi-modal austenite grain-size distribution can lead to the continuous martensitic transformation in a wide range of strains that

result in higher ductility during tensile test [14]. Although the mechanisms for higher ductility in UFG/NG bimodal austenitic stainless steels have been studied before [14], the reason for the formation of a bimodal grain-size distribution during thermomechanical processing is not yet clear. Therefore, in this paper, we focus on the relation between strain induced martensitic transformation and the formation of bimodal austenite structure in AISI 304L stainless steel, through characterization of the martensitic transformation by using Transmission Electron Microscopy (TEM) and nanoindentation experiments.

2. Material and methods

A commercial AISI 304L stainless steel, in the form of a sheet with thickness 10 mm, was used as the initial material. Several specimens with dimensions of 100 mm × 40 mm were cut from the initial sheet for cold rolling. Cold rolling was performed to different reductions from 70% to 93% at temperature of -15 $^{\circ}$C in a mixture of ethanol and ice with interpass cooling. The cold rolled samples were subjected to annealing at 700 $^{\circ}$C for 300 min.

A ferritescope (Helmut Fischer GmbH, model MP30E) was used for the quantification of the ferromagnetic α′-martensite phase during rolling process. The device was calibrated with δ-ferrite standard samples and the results were converted into α′-martensite contents with a correlation factor of 1.7 [15]. X-Ray Diffraction (XRD) analysis was done to characterize the phases in the rolled sample. A Field-Emission Scanning Electron Microscope (Hitachi S4800) and Transmission Electron Microscope (FEI Tecnai G2 20 Scanning TEM) examinations were employed to follow the martensitic transformation in the rolled sample and to characterize final austenite grain structure. Two-beam condition was used to image the dislocation debris of the

rolled martensite and dislocation densities were evaluated. Nanoindentation tests were performed using an Agilent G200 Nanoindenter equipped with a Berkovich tip in the load control mode with the maximum load of 10 mN. Tension tests were also performed at room temperature according to ASTM E8 standard using a tensile machine (Hounsfield H50ks) at a crosshead speed of 1mm/min.

3. Results and discussion:

Fig. 1(a) shows XRD patterns of the as-received and rolled samples after different rolling reductions. According to the XRD results, the as-received sample is fully austenitic containing γ (111), γ (200), γ (220) and γ (311) peaks. Increasing the rolling reduction leads to gradual transformation of austenite into α' martensite, so that there are just three peaks of α' martensite, namely, α' (110), α' (200), α' (211), after 80% cold rolling. The results of ferritescope show that 55% cold roll reduction is the martensite saturation state, so that around 98 vol.% of the sample is fully covered by martensite at this stage. Figs. 1(b,c) show the SEM micrographs of the 15% and 35% cold rolled samples, respectively. The morphology of martensite after 15% reduction is lathy and this breaks down into finer lathes after 35% rolling reduction. Also, the density of lath type martensite is increased by further rolling.

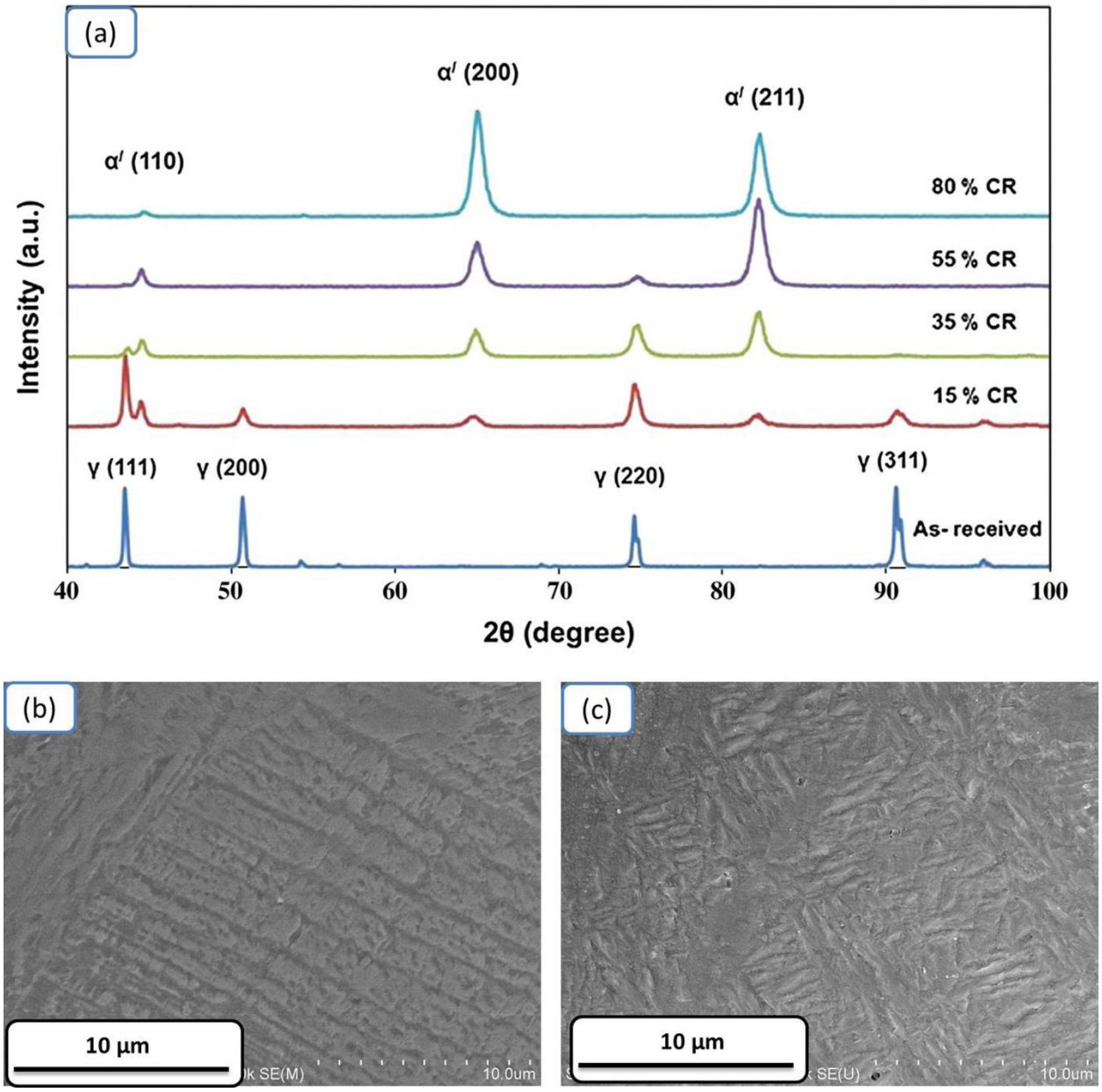

Fig. 1: XRD patterns of the as-received and cold rolled AISI 304L stainless steel (a) and SEM micrographs of the 15% (b) and 35% (c) cold rolled samples

Fig. 2 shows TEM micrographs of the 5% rolled sample. Three different α′ martensite nucleation mechanisms was observed for this sample. Fig. 2(a,b) show that the α′ martensite nucleates at the

intersections of the nano-scale shear bands. The TEM images showing the second mechanism can be seen in Fig. 2(c,d). In this case the α' martensite nucleates in a single shear band without any intersection. It seems that the growth of martensite occurs through repeated nucleation of nuclei and coalescence of such nuclei into long lathes, which is consistent with the results of other studies [16]. This growth mechanism is more evident in the TEM image of Fig. 2(c). The third mechanism was identified as the nucleation of martensite in an intersection between a grain boundary and a shear band (Fig. 2(e)). In our experiments, the second mechanism was identified as the most dominant since most of the martensite nuclei were formed by direct formation from single shear bands. Selected area diffraction showed that the shear band was a mechanical twin formed by rolling (Fig. 2(f)).

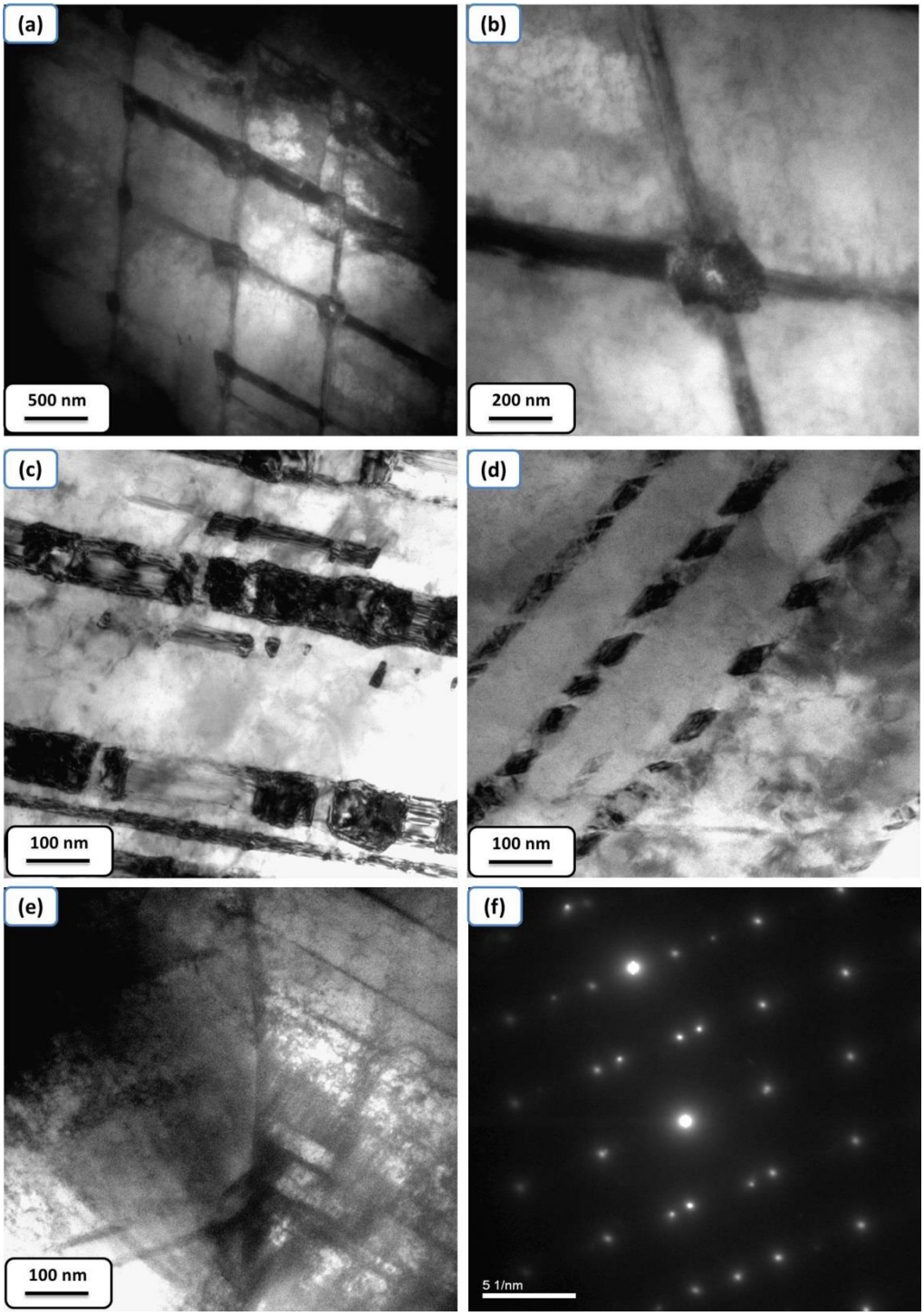

Fig. 2 : Nucleation of $\alpha^{/}$ martensite in 5% rolled sample at the (a and b) intersection of nano scale shear band (c,d) single shear band (e) Shear band – grain boundary intersection. (f) selected area diffraction pattern of a single shear band

Fig. 3 (a,b) show the TEM micrographs of the 35% and 55% cold rolled samples, respectively. The TEM image of the 35% cold rolled sample confirms the previously stated mechanism about the growth of α' martensite which is based on coalescence of nuclei. As stated previously, 55% cold rolling was identified as the saturation state where most (98%) of austenite transformed into martensite. Meanwhile, a few remaining austenite regions with the size of several hundred nanometers were still present (Fig. 3(b)), although the amount reaches to ~1% after 93% rolling reduction and so it should not have any considerable effect on the further events during annealing.

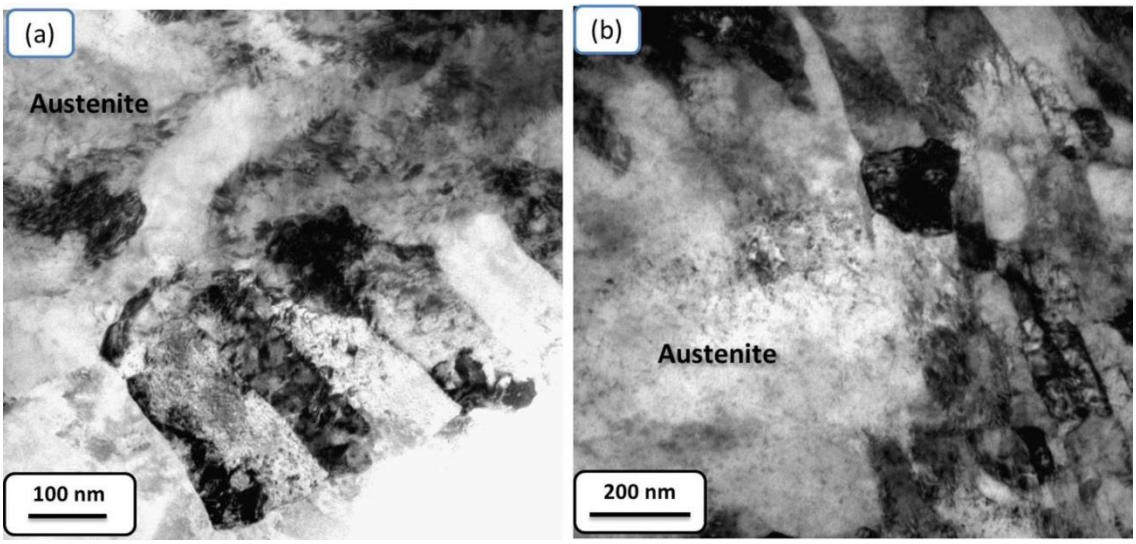

Fig. 3: TEM micrographs of the cold rolled sample after (a) 35% rolling (b) 55 % rolling reduction

Fig. 4(a) shows a low-magnification TEM image of the 60% cold rolled sample. The martensite lathes are elongated along the rolling direction, and their widths are measured to be around 100 nm. Although most of the martensite elongates completely along the rolling direction, there are

some areas near the prior austenite grain boundaries, such as the circled part in Fig. 4(a), where the martensite morphology is different from other areas. Higher-magnification inspection in fact shows that this area is still covered by lath type martensite, but the lathes are wider and less elongated. This means that the amount of deformation is not sufficient yet for the formation of finely structured martensite. It has been reported that higher reduction after reaching the saturation state can lead to finer austenite grains [6]. Cold deformation of martensite after attainment of the saturation state can destroy the structure leading to finer martensite, hence producing sufficient energy and nucleation sites for the subsequent reversion transformation to austenite to obtain UFG structure. Therefore, it seems that 60% cold-roll reduction is not sufficient yet to create suitable martensite morphology to obtain UFG austenite microstructure after annealing.

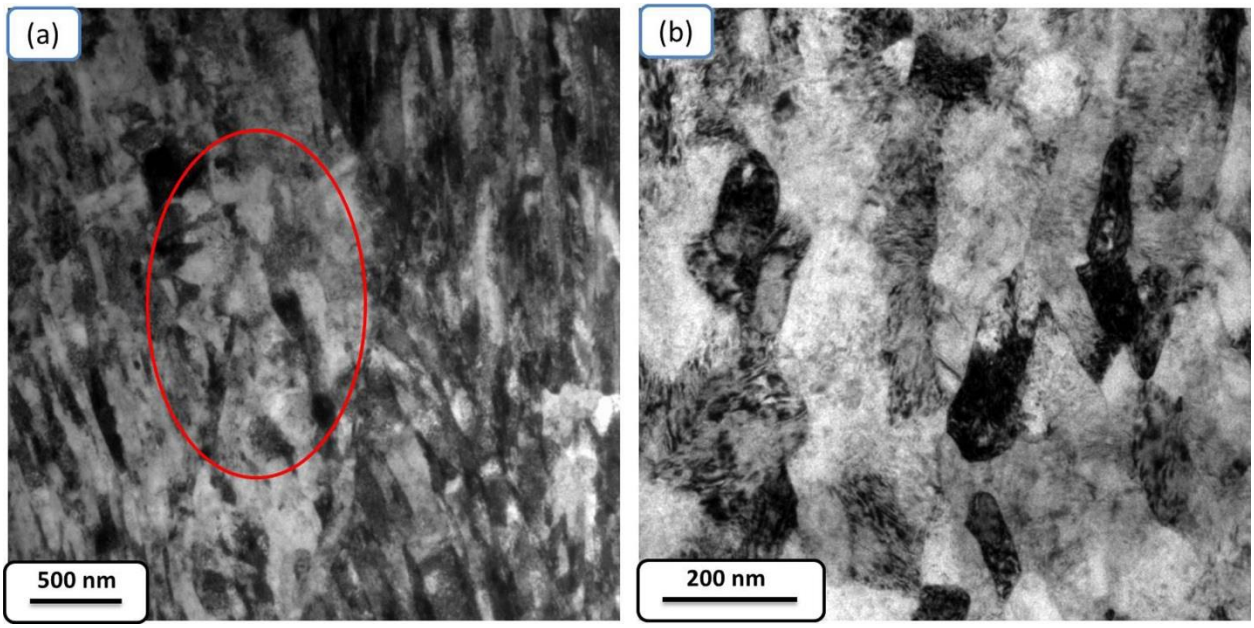

Fig. 4: (a) Low-magnification TEM micrograph of the 60% cold rolled sample, (b) higher-magnification micrograph of the area circled in (a).

TEM Micrographs of a sample cold rolled to 80% reduction are shown in Fig. 5. Both lath-type martensite (Fig. 5 (a)) and deformation-cell type martensite (Fig.5 (b)) are visible in different regions of the microstructure. It should be noted that lath martensite is characterized by spot-like diffraction patterns while dislocation-cell type martensite with high dislocation densities would yield a ring type diffraction pattern [17-19]. Further rolling after the saturation state can lead to breaking up of the lath-structured martensite into smaller lathes and finally reaching the dislocation-cell type martensite [17-19]. The size of regions exhibiting dislocation-cell type martensite were found to be around 1 μm^2 or higher in other areas. It is reported that the formation of slip bands during further rolling can be a reason for the change from lath to dislocation-cell type of martensite [20-21]. As stated by Misra et al. [18], these two types of martensite are always present simultaneously in the rolled samples after the saturation state, and further rolling only changes their volume fractions. It was reported that under the same annealing time, the amount of reversed austenite is always higher in the samples with higher cold-roll reduction [19]. It means that there are more potential nucleation sites in dislocation-cell type martensite and so the presence of this type of martensite is necessary for obtaining nano/ultrafine austenite grains during the subsequent reversion annealing treatment [19]. The average width of the martensite lathes in the 80% rolled sample is measured as 60 nm. It should be noted that the lath martensite in the 80% rolled sample is finer than that in the 60% rolled sample. A bright-field TEM image of a martensite lath in the 80 % rolled sample under a two-beam condition is shown in Fig. 5 (c). From the observed spacing between dislocations, the dislocation density inside the lath is estimated as 5×10^{15} m^{-2}. Similarly, the dislocation density of the lathes in the 60% rolled sample is estimated as about 2×10^{15} m^{-2}. Therefore, the lathes of the 80% rolled

sample are characterized by their finer width, although the dislocation density is nearly similar to that of the 60% rolled sample.

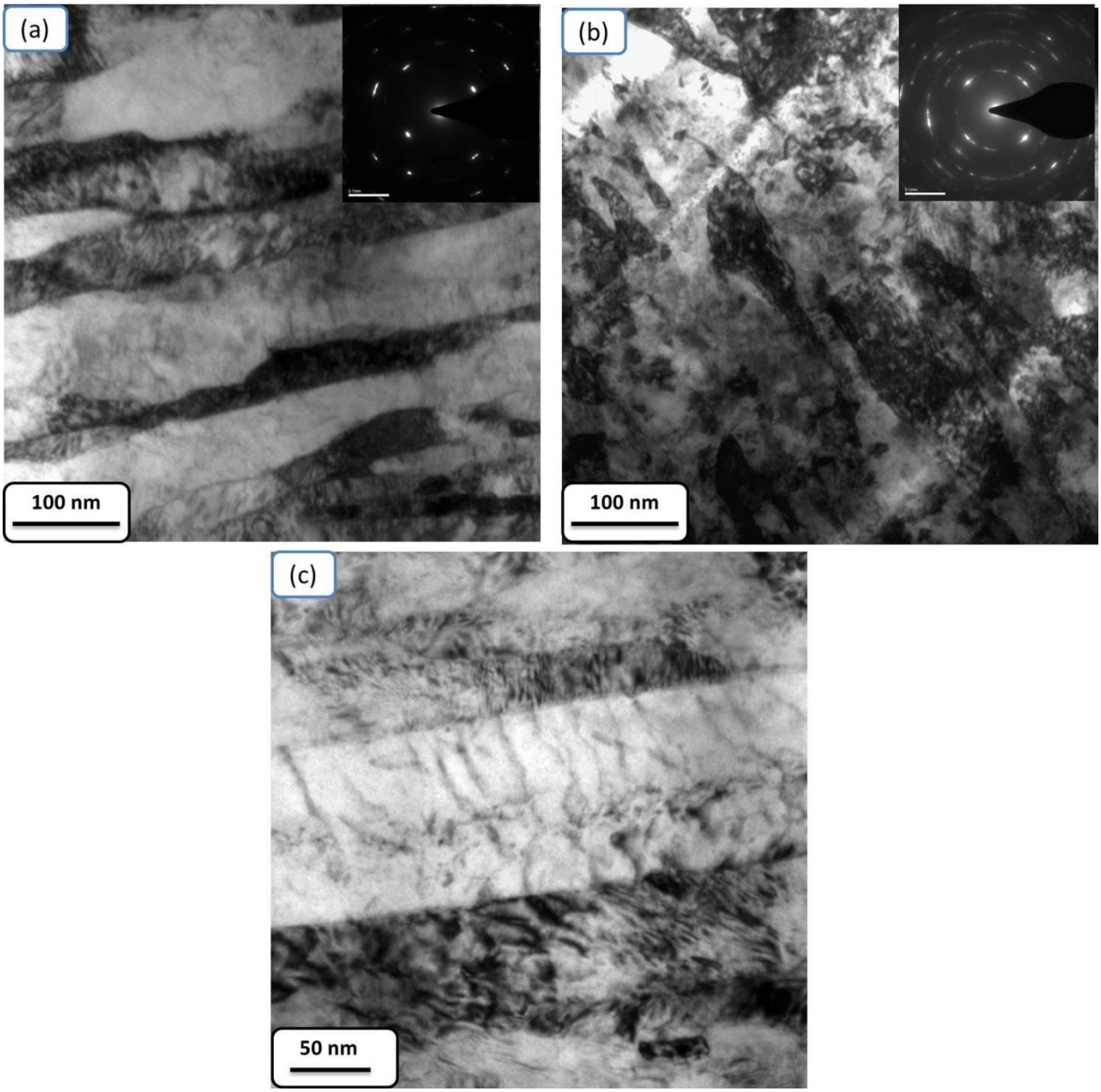

Fig. 5: TEM images of the 80% cold rolled sample, showing (a) lath type martensite, (b) dislocation-cell type martensite. (c) Bright-field TEM image of a martensite lath under two-beam condition.

Nanoindentation tests were carried out on 5 × 5 arrays with 4 times repetition in the samples after reaching the saturation state, in order to follow the hardness changes with increasing the amount of dislocation-cell type martensite. The distance between two neighboring indents was selected as 15 μm, while the typical size of the indents was around 1.2 μm. Surface roughness is a very important parameter affecting the accuracy of nanoindentation results [22-24], and for this reason, atomic force microscopy (AFM) scanning in contact mode was performed to study the surface roughness of the samples before the nanoindentation tests (Fig. 6). According to ISO 14577, the surface roughness should be less than 5% of the maximum penetration depth for a hardness error of 10% or less. The average roughness of the present samples was found to around 10 nm, which is small enough compared to the maximum penetration depth in the nanoindentation tests (larger than 200 nm).

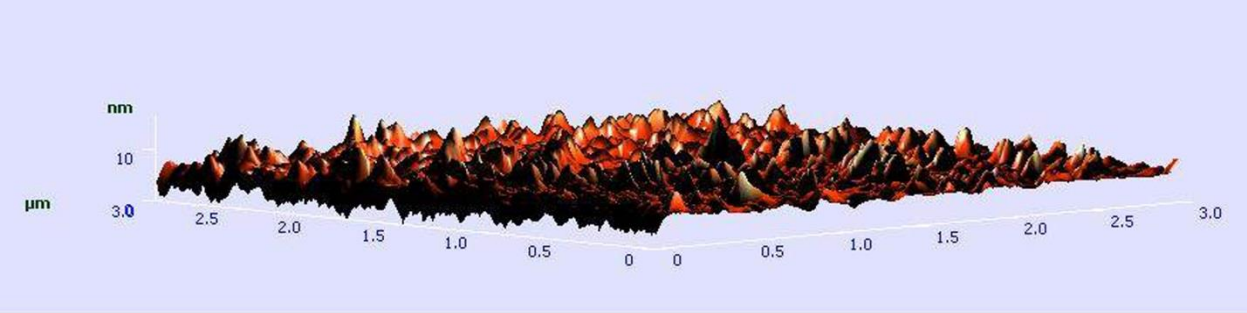

Fig. 6: AFM image of the 80% rolled sample before nanoindentation test

Fig. 7 (a) shows typical load-displacement curves from nanoindentation tests of the 60%, 70% and 80% cold rolled samples. Frequency plots of the hardness measured using the Oliver-Pharr method [25] are also shown in Fig. 7 (b). The average hardness of the 60%, 70% and 80% rolled sample was determined as 7.15, 8.5 and 10.1 GPa, respectively. Based on the TEM results, the progressive increase in the hardness of the rolled samples after the saturation state can be

related to the simultaneous effects of a reduction in the lathes size and the formation of dislocation-cell type martensite regions. It should be noted that the scattering of hardness data in the 80% rolled samples is larger than that of the 60% rolled sample, namely, the standard deviation of the hardness is 1.3 GPa and 0.4 GPa for these two samples, respectively. Such scattering can also confirm the existence of some microstructural regions with higher hardness, which are likely the dislocation-cell type martensite regions.

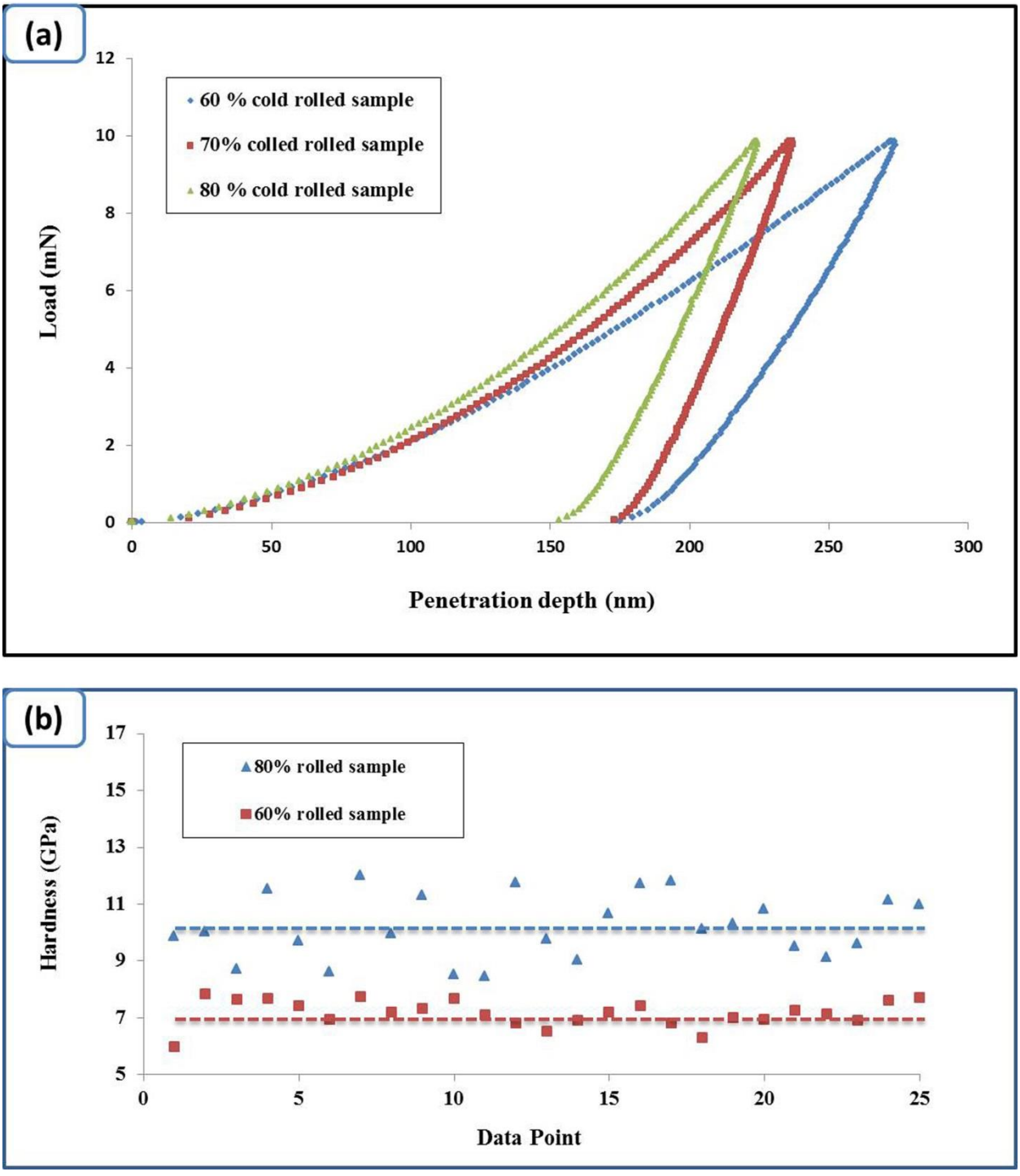

Fig. 7: (a) Typical Load-displacement curve of the 60%, 70% and 80% rolled samples (b) Frequency plot of the hardness of the 60% and 80% rolled samples

Fig.8 (a,b) show the SEM images of the 80% cold rolled sample after annealing at 700 °C for 300 min. The microstructure consists of reverted austenite with a bimodal grain-size distribution, which comprises smaller grains with an average grain size of 300 nm surrounded by larger grains with an average grain size of 1 μm. Image analysis showed that the bimodal microstructure is composed of ~60% larger grains and 40% smaller grains. It has been reported [26-27] that whether the reversion mechanism of martensite to austenite during annealing is shear-controlled or diffusional depends on both the chemical composition and annealing temperature. As stated by Tamimura et al. [26], calculation of the Gibbs free energy change during the $\alpha' \rightarrow \gamma$ reversion transformation can help to determine the reversion mechanism. Their results showed that the critical driving force required for complete shear reversion is about – 500 J/mol which is independent of the chemical composition of the alloy. The following equation for the Gibbs free energy change $\Delta G^{\alpha' \rightarrow \gamma}$ during the martensite to austenite reversion in ternary Fe-Cr-Ni alloys was suggested [26]:

$$\Delta G^{\alpha' \rightarrow \gamma} \text{ (J/mol)} = 10^{-2}\, \Delta G_{Fe}^{\alpha' \rightarrow \gamma} (100 - \text{Cr} - \text{Ni}) - 97.5\,\text{Cr} + 2.02\,\text{Cr}^2 - 108.8\,\text{Ni} + 0.52\,\text{Ni}^2 - 0.05\,\text{Cr Ni} + 10^{-3}\, T\,(73.3\,\text{Cr} - 0.67\,\text{Cr}^2 + 50.2\,\text{Ni} - 0.84\,\text{Ni}^2 - 1.51\,\text{Cr Ni}) \quad \text{eq.1}$$

where $\Delta G_{Fe}^{\alpha' \rightarrow \gamma}$ is the free energy change in pure iron, *T* is the temperature in Kelvin and Cr and Ni represent the mass % of the two elements. However, Somani et al. [28] have shown that this equation does not provide acceptable predictions in commercial austenitic stainless steels containing alloying elements other than chromium and nickel, which are neglected. They suggested using Cr_{eq} and Ni_{eq} rather than the simple mass % of Cr and Ni in the above equation, which can be determined as

$$Cr_{eq} = Cr + 4.5\,Mo \quad \text{eq.2}$$

Ni_{eq} = Ni + 0.6 Mn + 20 C +4N – 0.4Si eq.3

Using the above equations, $\Delta G^{\alpha' \rightarrow \gamma}$ was finally calculated as -556 J/mol using Cr_{eq} , Ni_{eq} and thermodynamic data reported by Kaufman et al. [29] at the annealing temperature of 973 K. This value of $\Delta G^{\alpha' \rightarrow \gamma}$ suggests that the reversion mechanism should be shear controlled at this temperature.

As stated by Tomimura et al. [26], the microstructure of the reversed austenite produced completely by the shear mechanism depends on the morphology of the martensite before the reversion, while no strong correlation of the microstructures before and after the reversion transformation exists in the diffusion controlled mechanism because the austenite nucleates and grows randomly. In other words, the occurrence of the shear mechanism during reversion treatment can give rise to a microstructural similarity between the deformation induced martensite and the reversed austenite. Therefore, the occurrence of a bimodal grain-size structure after reversion annealing can be attributed to the lath and dislocation-cell type martensite in the rolled sample. SEM micrographs of the 70% and 93% rolled and annealed samples are shown in Fig. 9(a,b). In both samples, a weak bimodal structure was still observed. Two considerable trends can be found with increasing rolling reduction before annealing. First, the average austenite grain size decreased with increasing rolling reduction, i.e. it reached 1.3 μm, 0.65 μm and 0.3 μm after 70%, 80% and 93% rolling followed by annealing. Secondly, the average area percentage covered by smaller grains in the bimodal structure increased with increasing rolling reduction, namely, it reached 20%, 40% and 75% after 70%, 80% and 93% rolling followed by annealing. The occurrence of shear controlled reversion mechanism indicates that the microstructural difference between these samples is due to the change in the amounts of lath type and dislocation-cell type martensite on further rolling reduction, and this supports the previous

claim that these two types of martensite play an important role on the final bimodal grain size after annealing. It should be noted that the formation of equiaxed austenite grains after the reversion treatment is related to a sufficient extent of cold rolling before annealing. The effect of prior cold work content on the reverted austenite shape was previously studied by Takaki et al. [20] on a laboratory melted 18Cr-8.5Ni clean steel. They reported that under insufficient cold rolling of $\sim$ 50 %, reverted austenite nucleates within large martensite blocks, and after full reversion, a stratum structure of austenite lathes and blocks is produced. Meanwhile when the cold roll reduction is sufficient at 90%, the martensite morphology is fine enough so that austenite grains nucleate in random directions and finally form equiaxed grains with grain size close to 1 μm. The TEM images of Fig. 8 (c-d) also show that the microstructure after annealing exhibits high dislocation density which can confirm the shear controlled reversion transformation, as the diffusion controlled mechanism should be associated with very low dislocation density in the reversed austenite which forms from nucleation and growth.

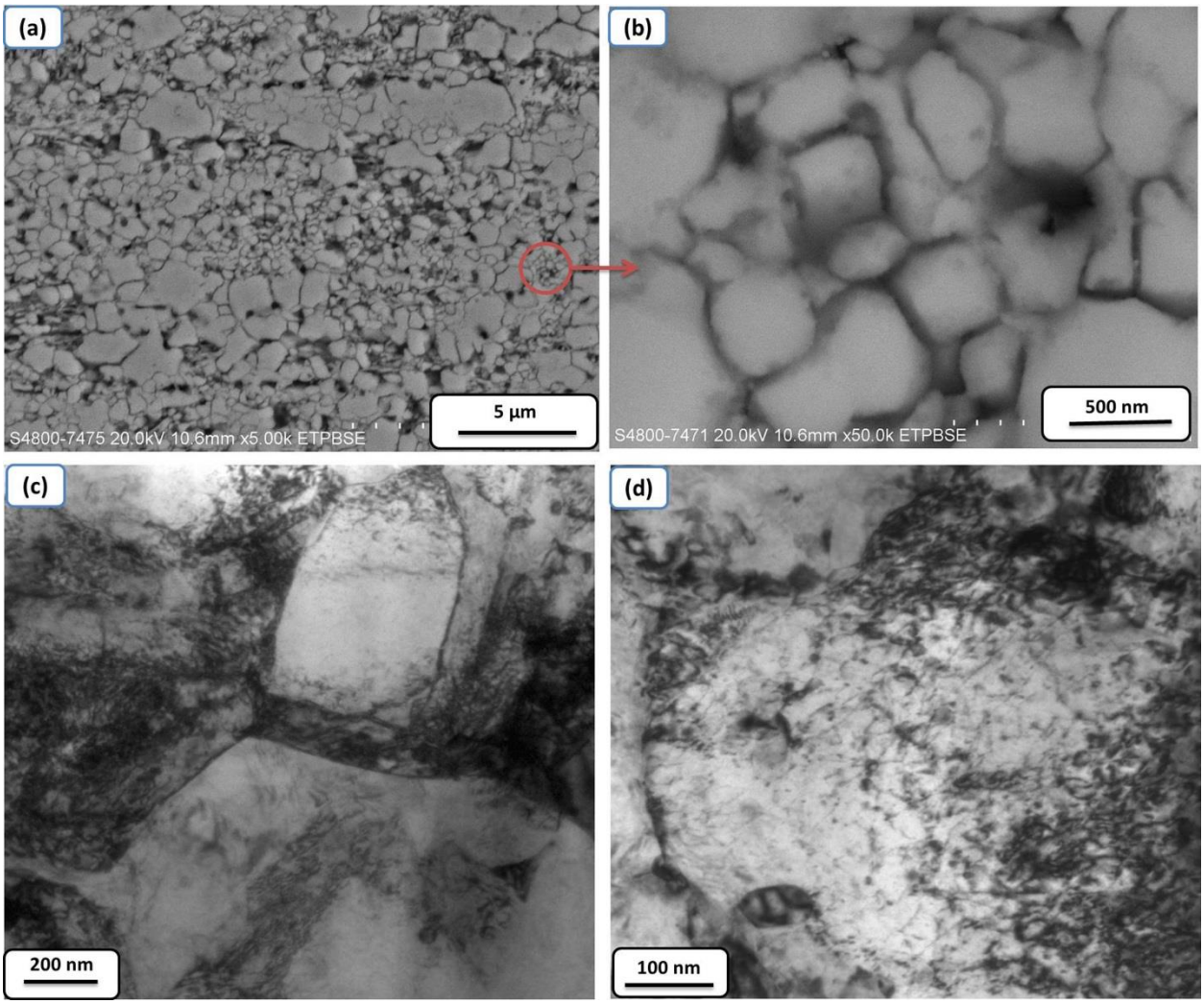

Fig. 8 : HRSEM (a, b) and TEM micrograph (c,d) of the 80% rolled and annealed sample with UFG bimodal grain-size distribution

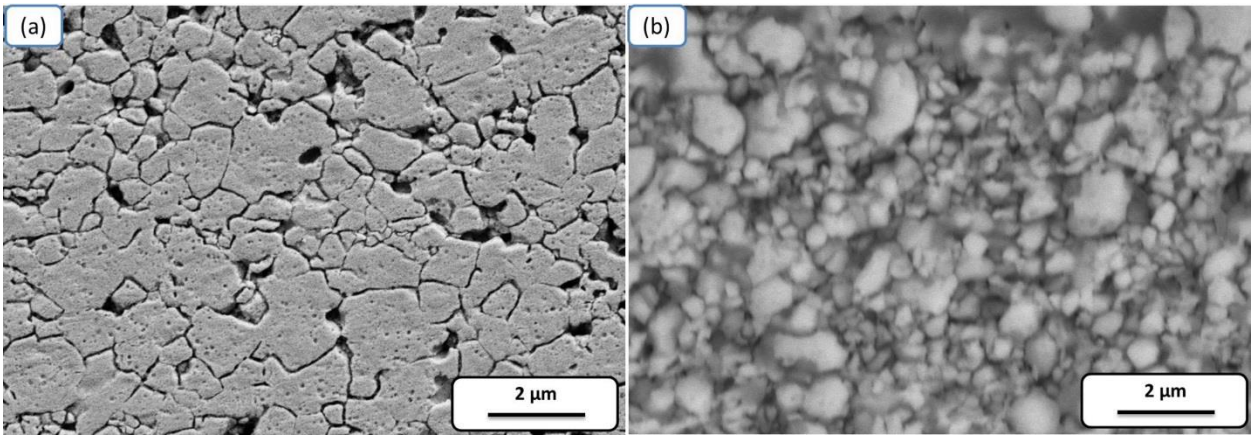

Fig. 9: HRSEM image of the 70% (a) and 93% (b) rolled and annealed samples

Fig. 10(a) shows the engineering stress-engineering strain curve of the 80% and 93% rolled and annealed samples. The true stress-true strain curves in the plastic region of the two samples are also plotted in Fig. 10(b), which shows that the curves in the plastic regime are nearly linear in both samples, which means that the work hardening rates are roughly constant up to the point of rupture. The measured work hardening rate of the 80% rolled and annealed sample (1672 MPa) is only slightly higher than that of the 93% rolled and annealed sample (1574 MPa). The 80% rolled and annealed sample, which had a clear bimodal structure, exhibited a yield stress of 720 MPa, ultimate tensile stress of 920 MPa, and total elongation of 47 %. However, the 93% rolled and annealed sample showed higher yield stress and UTS with lower ductility. Another important difference between these two samples is a considerably lower uniform elongation in the 93% rolled and annealed sample. It seems that the main reason for uniform elongation drop in the 93% rolled and annealed sample is the change of the austenite grain structure towards a mono-modal structure. As stated previously, increasing in the rolling reduction can lead to an increase in the amount of dislocation-cell type martensitic regions which

finally transform into small austenite grains of around 300 nm during the reversion annealing. This result is consistent with the work of Hedayati et al. [5], who reported that the uniform elongation of a mono-modal AISI 304L stainless steel with an average grain size of 330 nm is around 20 % without any strain hardening. The occurrence of extensive uniform deformation during tensile testing of the present bimodal structured UFG 304L steel can be ascribed to the continuity of martensitic transformation over a wide range of strains. It is well known that the stability of austenite increases with decreasing grain size in both thermally and mechanically activated transformations. In UFG austenite with grain size of 1 μm or less, it has been reported that a large chemical driving force is required for the nucleation of single-variant martensite within a grain during subzero treatment [30]. In addition, it was found that grain refining down to the nanometric scale can lead to a significant restriction in the formation of strain induced martensite during indentation [31]. In fact, at the beginning of a tensile test when the strain is small, martensitic transformation occurs in larger austenite grains, and this continues in the finer grains as strain increases. Therefore, the existence of a bimodal structure with different grain sizes can lead to a higher ductility and more uniform elongation during a tensile test. Fig.10 (c,d) show the fracture morphology of the 80% and 93% rolled and annealed samples. It is clearly seen that the fracture surfaces of the both specimens contained many deep dimples homogeneously distributed like honeycombs. The main difference between these two fracture surfaces, however, is the dimple size which is significantly smaller after higher rolling reduction. In addition, some shear dimples were present in the 93% rolled and annealed sample. Therefore, it can be concluded that the fracture mode of the both samples is ductile in nature.

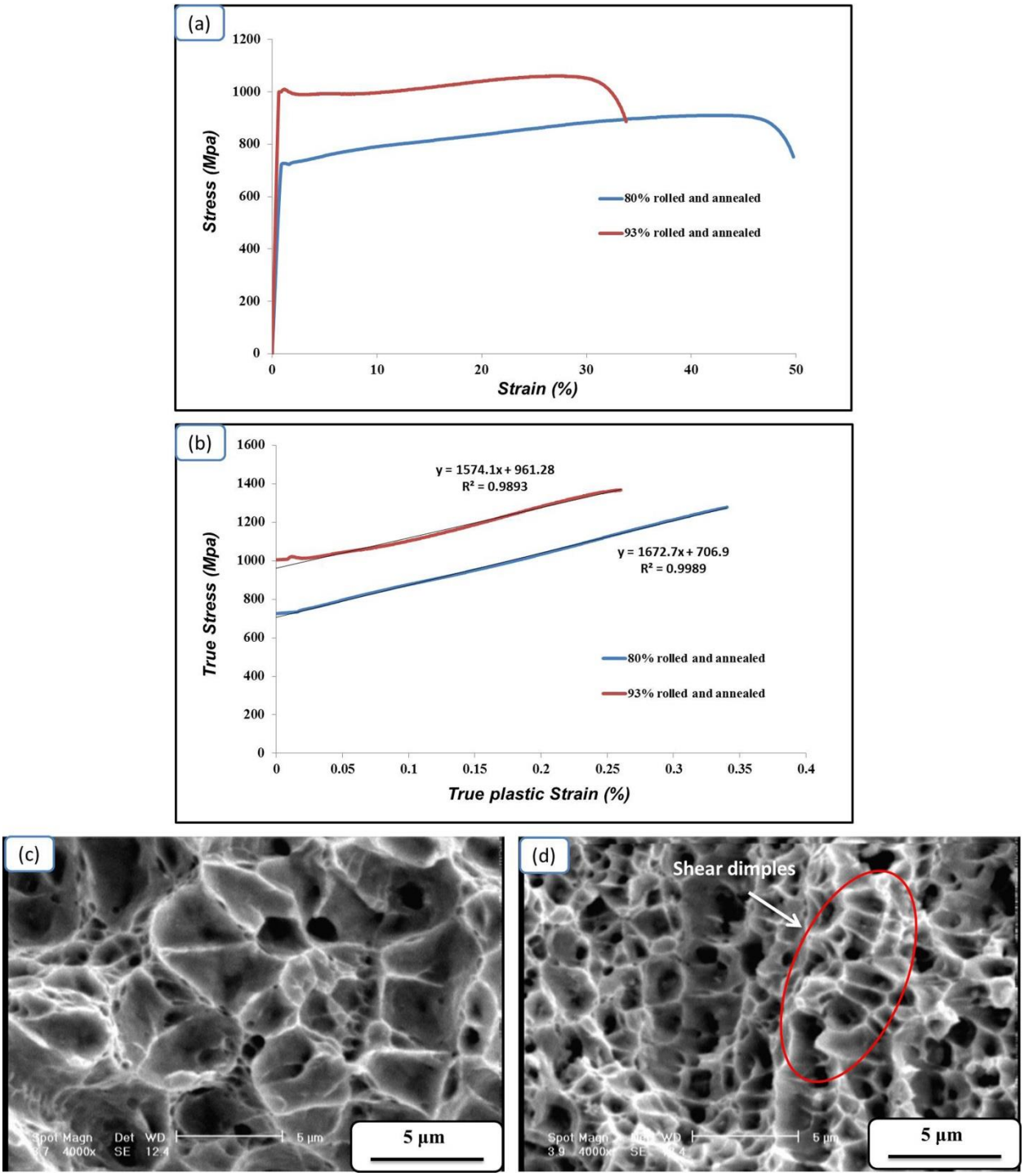

Fig. 10: (a) Engineering stress-engineering strain curve and (b) True stress- true plastic strain curve of the 80% and 93% rolled and annealed samples, fracture surface morphology of the 80% c) and 93% (d) rolled and annealed samples

4. Conclusions

The effects of martensitic transformation during cold rolling of an AISI 304L stainless steel on the resultant austenite grain structure after reversion annealing were studied. Important findings are as follow:

- An ultrafine-grained 304L austenitic stainless steel with bimodal grain-size distribution was successfully produced using a combination of cold rolling (80% reduction) and annealing (700 ^{0}C for 300 min).
- After 55% cold rolling, the structure was almost fully martensitic. In the 60% cold rolled sample the martensite morphology was full of the lath type with an average lath width of around 100 nm. The existence of wider and shorter lathes in some regions confirmed that the rolling reduction was not sufficient yet for the formation of finely structured martensite. Further rolling after 60% reduction caused the formation of both lath and dislocation-cell type martensite.
- Calculation of the Gibbs free energy change during the reversion treatment showed that the reversion mechanism is shear controlled at the annealing temperature. The occurrence of the shear controlled mechanism results in the microstructural similarity between the deformation martensite and reverted austenite. As a result of the existence of both types of martensite, different austenite grain sizes were formed.
- 80% rolled and annealed sample showed a bimodal structure which comprises smaller grains with an average grain size of 300 nm surrounded by larger grains with an average grain size of 1 μm. Increasing the rolling reduction to 93% followed by annealing caused the grain structure to change towards a mono-modal like structure with mostly smaller grains of around 300 nm.

- The 80% rolled and annealed state with bimodal grain-size distribution showed a combination of high strength and ductility, and a tensile elongation of 47%. Meanwhile, the 93% rolled and annealed state showed high strength of 1 GPa, but the ductility, especially tensile elongation, is significantly lower.

5. References

[1] R.Nafar Dehsorkhi, S.Sabooni, F.Karimzadeh, A.Rezaeian, M.H.Enayati, "The effect of grain size and martensitic transformation on the wear behavior of AISI 304L stainless steel", Material and design, Vol.64, (2014), 56-62.

[2] S.Sabooni, F.karimzadeh, M.H,Enayati, " Thermal stabillity study of ultrafine grained 304L stainless steel produced by martensitic process", Journal of materials engineering and performance, Vol 23(5), (2014), pp 1665-1672.

[3] A. Momeni, S.M. Abbasi , Repetitive Thermomechanical Processing towards Ultra Fine Grain Structure in 301, 304 and 304L Stainless Steels, J. Mater. Sci. Technol., 2011, Vol. 27(4), 338-343.

[4] V.S.A. Challa, X.L. Wan, M.C. Somani, L.P. Karjalainen, R.D.K. Misra, Strain hardening behavior of phase reversion-induced nanograined/ultrafine-grained (NG/UFG) austenitic stainless steel and relationship with grain size and deformation mechanism, Materials Science and Engineering A, Vol. 613, (2014), 60–70.

[5] Ali Hedayati, Abbas Najafizadeh, Ahmad Kermanpur, Farnoosh Forouzan, The effect of cold rolling regime on microstructure and mechanical properties of AISI 304L stainless steel, Journal of Materials Processing Technology, Vol. 210, (2010), 1017–1022.

[6] Farnoosh Forouzan, Abbas Najafizadeh, Ahmad Kermanpur, Ali Hedayati, Roohallah Surkialiabad, Production of nano/submicron grained AISI 304L stainless steel through the martensite reversion process, Materials Science and Engineering A, Vol. 527, (2010), 7334–7339.

[7] R.D.K. Misra, S. Nayak, S.A. Mali, J.S. Shah, M.C. Somani, L.P. Karjalainen, On the Significance of Nature of Strain-Induced Martensite on Phase-Reversion-Induced Nanograined/Ultrafine-Grained Austenitic Stainless Steel, Metallurgical and Materials Transactions A, Vol.41(1), (2010), pp 3-12 .

[8] S. Rajasekhara, P.J. Ferreira, L.P. Karjalainen, A. Kyröläinen, Hall–Petch Behavior in Ultra-Fine-Grained AISI 301LN Stainless Steel, Metallurgical and Materials Transactions A, Vol. 38(6), (2007), pp 1202-1210 .

[9] E. Ma, Eight Routes to Improve the Tensile Ductility of Bulk Nanostructured Metals and Alloys, JOM, Vol. 58(4), 2006, , pp 49-53.

[10] D. Farkas, H. Van Swygenhoven, P.M. Derlet, Intergranular fracture in nanocrystalline metals, Phy. Rev. B, Vol. 66, (2002), 060101.

[11] Q.M. Wei, D. Jia, K.T. Ramesh, E. Ma, Evolution and microstructure of shear bands in nanostructured Fe , Appl. Phys. Lett., Vol. 81, (2002), 1240

[12] Yury Gogotsi, Nanomaterials Handbook, CRC Press, 2006.

[13] Y.M. Wang, E. Ma, Strain hardening, strain rate sensitivity, and ductility of nanostructured metals, Mater. Sci. Eng. A, Vol. 375–377, (2004), 46.

[14] B. Ravi Kumar, Dierk Raabe, Tensile deformation characteristics of bulk ultrafine-grained

austenitic stainless steel produced by thermal cycling, Scripta Materialia, Vol. 66 (2012) , 634–637.

[15] A. Rezaee, A. Kermanpur, A. Najafizadeh, M. Moallemi, H. Samaei Baghbadorani, Investigation of cold rolling variables on the formation of strain-induced martensite in 201L stainless steel, Material & design, Vol. 46, (2013), p 49–53.

[16] W.Sh.Lee, Ch.F. Lin, The morphologies and characterization of impact induced martensite in 304L stainless steel, Scripta Materialia, Vol. 43, (2000), 777-782.

[17] R.D.K. Misra, S. Nayak, S.A. Mali, J.S. Shah, M.C. Somani, L.P. Karjalainen, Microstructure and Deformation Behavior of Phase-Reversion-Induced Nanograined/Ultrafine-Grained Austenitic Stainless Steel, Metallurgical and Materials Transactions A, Vol. 40 (10), 2009, pp 2498-2509 .

[18] R. D. K. Misra, J. S. Shah, S. Mali, P. K. C. Venkata Surya, M. C. Somani, L. P. Karjalainen, Phase reversion induced nanograined austenitic stainless steels: microstructure, reversion and deformation mechanisms, Materials Science and Technology, Vol.29(10), (2013), pp. 1185-1192.

[19] S. Rajasekhara, L.P. Karjalainen, A. Kyröläinen, P.J. Ferreira, Microstructure evolution in nano/submicron grained AISI 301LN stainless steel, Materials Science and Engineering A, Vol. 527, (2010), 1986–1996.

[20] S.Takaki, K.Tamimura, S.Ueda Effect of Pre-cold-working on Diffusional Reversion of Deformation Induced Martensite in Metastable Austenitic Stainless Steel, ISIJ International. Vol. 34(6), (1994), pp. 522-527

[21] Kouki TOMINIURA, Yuuji KAWAUCHI, Setsuo TAKAKI, Youichi TOKUNAGA, Effect of Prior Deformation on Grain Refining Process of Martensitic Shear Reversion in Metastable Austenitic Stainless Steel, Tetsu-to-Hagané, Vol. 77(9), (1991), p 1519.

[22] Nagy, P. M.; Kükemezey, I. Istvan; Kassavetis, S.; Berke, P.; Delplancke-Ogletree, M.-P.; Logothetidis, S., The Effect of Roughness on Nanoindentation Results, Nanoscience and Nanotechnology Letters, Vol. 5(4), (2013), 480-483

[23] K.-D. Bouzakisa, N. Michailidisa, S. Hadjiyiannisa, G. Skordarisa, G. Erkens, The effect of specimen roughness and indenter tip geometry on the determination accuracy of thin hard coatings stress–strain laws by nanoindentation, Materials Characterization, Vol. 49, (2003), 149–156.

[24] Yang Xia, Maxence Bigerelle, Julie Marteau, Pierre-Emmanuel Mazeran, Salima Bouvier andAlain Iost, Effect of surface roughness in the determination of the mechanical properties of material using nanoindentation test, scanning, Vol. 36(1), (2014), 134-149.

[25] W.C.Oliver and G.M.Pharr, Journal of Materials Research, An improved technique for determining hardness and elastic modulus using load and displacement sensing indentation experiments, Vol.7, (1992) , 1564-1583.

[26] K. Tomimura, S.Takaki and Y.Tokunaga, Reversion mechanism from Deformation Induced Martensite to austenite in Metastable Austenitic Stainless Steels, ISIJ, Vol. 31(12), (1991), 1431-1437.

[27] P.Behjati, A.Kermanpur, A.Najafizadeh, H. Samaei Baghbadorani, Effect of annealing temperature on nano/ultrafine grain of Ni-free austenitic stainless steel, Materials Science&Engineering A, 592, (2014), 77–82.

[28] M.C.Somani, P.Juntunen, L.P.Karjalainen, R.D.K.Misra, A.Kyrolainen, Enhanced Mechanical Properties through Reversion in Metastable Austenitic Stainless Steels, Metallurgical and materials transaction A, Vol. 40A, (2009), 729-744.

[29] L. Kaufman, E.V.Clougherty, R.J.Weiss, The lattice stability of metals—III. Iron, Acta Metallurgica, Vol. 11, (1963), 323–335.

[30] Setsuo Takaki, Kazuhiro Fukunaga, Junaidi Syarif,Toshihiro Tsuchiyama, Effect of Grain Refinement on Thermal Stability of Metastable Austenitic Steel, Materials Transactions, Vol. 45(7), (2004), 2245 -2251

[31] S. Sadeghpour, A.Kermanpur, A.Najafizadeh, Investigation of the effect of grain size on the strain-induced martensitic transformation in a high-Mn stainless steel using nanoindentation, Materials Science & Engineering A, Vol. 612, (2014), 214–216.